K isotopes as a tracer for continental weathering and geological K cycling

Shilei Li (李石磊)[a,b], Weiqiang Li[c,1], Brian L. Beard[d,e], Maureen E. Raymo[b], Xiaomin Wang (王小敏)[c], Yang Chen (陈旸)[a], and Jun Chen[a]

[a]Ministry of Education, Key Laboratory of Surficial Geochemistry, School of Earth Sciences and Engineering, Nanjing University, Nanjing 210023, China; [b]Lamont-Doherty Earth Observatory, Columbia University, Palisades, NY 10964; [c]State Key Laboratory for Mineral Deposits Research, School of Earth Sciences and Engineering, Nanjing University, Nanjing 210093, China; [d]Department of Geoscience, University of Wisconsin–Madison, Madison, WI 53706; and [e]NASA Astrobiology Institute, University of Wisconsin–Madison, Madison, WI 53706

Edited by Mark H. Thiemens, University of California at San Diego, La Jolla, CA, and approved March 22, 2019 (received for review June 30, 2018)

The causal effects among uplift, climate, and continental weathering cannot be fully addressed using presently available geochemical proxies. However, stable potassium (K) isotopes can potentially overcome the limitations of existing isotopic proxies. Here we report on a systematic investigation of K isotopes in dissolved load and sediments from major rivers and their tributaries in China, which have drainage basins with varied climate, lithology, and topography. Our results show that during silicate weathering, heavy K isotopes are preferentially partitioned into aqueous solutions. Moreover, $\delta^{41}K$ values of riverine dissolved load vary remarkably and correlate negatively with the chemical weathering intensity of the drainage basin. This correlation allows an estimate of the average K isotope composition of global riverine runoff ($\delta^{41}K = -0.22‰$), as well as modeling of the global K cycle based on mass balance calculations. Modeling incorporating K isotope mass balance better constrains estimated K fluxes for modern global K cycling, and the results show that the $\delta^{41}K$ value of seawater is sensitive to continental weathering intensity changes. Thus, it is possible to use the $\delta^{41}K$ record of paleo-seawater to infer continental weathering intensity through Earth's history.

continental weathering | K isotopes | rivers | fractionation | K cycling

Silicate weathering acts as a major sink for atmospheric CO_2 in the long-term geological carbon cycle (1–3). Tracing secular variations in silicate weathering can therefore enhance our understanding of the evolution of atmospheric CO_2 and Earth's climate (1, 4, 5). Reconstructing silicate weathering processes through Earth's history requires robust and sensitive proxies. Commonly used silicate weathering proxies include Sr, Os, and Li isotopes. For example, it has been proposed that the increase in $^{87}Sr/^{86}Sr$ ratios in Cenozoic seawater during the past 40 My was caused by an increase in silicate weathering rates in response to continental uplift (2). However, the increase in seawater $^{87}Sr/^{86}Sr$ can also be attributed to the dissolution of vein calcite in granitic rocks that contain abundant radiogenic Sr (6, 7), thus weakening the link between seawater Sr isotope records and silicate weathering. Similarly, the increase in seawater $^{187}Os/^{188}Os$ (8) during the Cenozoic has been explained by increased continental weathering rates; however, given that Os is hosted mainly in anoxic marine sediments (9), seawater $^{187}Os/^{188}Os$ signatures should mainly reflect organic carbon flux (10, 11) and/or pyrite weathering (12), rather than silicate weathering rates. The Li isotope proxy is also ambiguous because the response of Li isotopes in riverine input to variations in weathering is not monotonic (13). Although δ^7Li values in detrital sediments (14) can be used to trace weathering intensity (WI), detrital sediments generally only record the regional weathering history (15) rather than providing a global integrated signal. Moreover, the Li isotopic composition of crustal materials is highly variable, meaning that the use of this proxy requires knowledge of the basin geology (14). Therefore, a new silicate weathering proxy that can overcome the limitations of existing isotopic tracers is needed.

Potassium (K) stable isotopes (^{39}K and ^{41}K) are ideal for tracing silicate weathering processes because ∼90% of K in riverine dissolved loads is derived from silicate weathering (16, 17). Moreover, K is a major element and its isotopic variations may be more directly coupled with the geological cycling of alkali elements, thus complementing the isotopic systems of trace elements such as Li and Rb. In addition, most igneous rocks (excluding volumetrically minor pegmatites and ultrapotassic rocks) have a narrow range of K isotopic compositions (18). High-precision $^{41}K/^{39}K$ measurements by multicollector inductively coupled plasma mass spectrometry allow identification of the K isotopic offset (0.6‰ in $^{41}K/^{39}K$) between igneous rocks and seawater (18–21). This implies that cycling of K between geological reservoirs is associated with significant K isotope fractionations that can be used to better understand the natural processes involving K fluxes. A recent study suggested a lack of K isotope fractionation during low-temperature alteration of basalt at the seafloor (22), although the samples were from only one ophiolite with debatable representativeness of altered oceanic crust. The K isotopic offset between igneous rocks and seawater may arise from the preferential incorporation of light K isotopes into clays during authigenic clay formation in marine sediments or K isotopic fractionation during chemical weathering on continents. K isotope behavior during silicate weathering, however, has not been studied in detail.

To understand how K isotopes fractionate during silicate weathering and to explore the possibility of utilizing K isotopes as a proxy for silicate weathering, we systematically measured K isotope ratios in river waters from major rivers in China and their tributaries, as well as river sediments from two small watersheds that drain granitic rocks. Although the sample set does not

Significance

The potassium stable isotope system is a powerful new geochemical tool for understanding continental weathering linked to Earth's climate. Potassium isotopes fractionate strongly during silicate weathering, and $\delta^{41}K$ values in riverine dissolved loads correlate with the silicate weathering intensity of drainage basins. We provide an estimate of the $\delta^{41}K$ value for the global riverine input into the oceans and demonstrate the sensitivity of $\delta^{41}K$ in seawater to the continental silicate weathering process.

Author contributions: S.L., W.L., Y.C., and J.C. designed research; S.L., W.L., and X.W. performed research; W.L. and B.L.B. contributed new reagents/analytic tools; S.L., W.L., B.L.B., and M.E.R. analyzed data; and S.L. and W.L. wrote the paper.

The authors declare no conflict of interest.

This article is a PNAS Direct Submission.

[1]To whom correspondence should be addressed. Email: liweiqiang@nju.edu.cn.

This article contains supporting information online at www.pnas.org/lookup/suppl/doi:10.1073/pnas.1811282116/-/DCSupplemental.

precisely represent global riverine runoff, the studied rivers cover large catchments with significant variations in climate, lithology, and topography. Thus, these data are ideal for investigating the behavior of K isotopes in river systems during the weathering of felsic continental crust.

Results and Discussion

A total of 54 samples including river waters (n = 38), bedrock (n = 2), and river sediment (n = 14) were analyzed. The majority of the river waters are from major Chinese rivers including the Changjiang (Yangtze), Yellow, Brahmaputra, Mekong, Xijiang, and Minjiang Rivers (*SI Appendix*, Fig. S1). Many of the studied rivers drain terrains that are characterized by high relief and dry climate (i.e., the Tibetan Plateau), which are located in typical "weathering-limited" regions. We also analyzed waters from low-lying rivers, including the Xijiang and Ganjiang Rivers. K isotopic compositions of the samples were analyzed using an established protocol (19, 23). K isotope data are reported using the delta notation ($\delta^{41}K = [(^{41}K/^{39}K)_{sample}/(^{41}K/^{39}K)_{standard} - 1] \times 1{,}000$) relative to the K standard National Institute of Standards and Technology (NIST) Standard Reference Material 3141a (19, 23), as recommended by ref. 21. Measured $\delta^{41}K$ values for riverine dissolved loads ranged from −0.44‰ to +0.12‰ (*SI Appendix*, Table S1), whereas $\delta^{41}K$ values in river sediments ranged from −0.74‰ to −0.48‰ (*SI Appendix*, Table S2).

Seasonal $\delta^{41}K$ Variations in Riverine Dissolved Loads. All but one of the rivers were sampled once. However, we did assess if this sampling approach yields valid estimates of the annual K isotope flux of a river, based on analyses of water samples from the Changjiang River. This river was sampled 11 times near Nanjing city, with samples taken at ∼30-d intervals (*SI Appendix*, Table S3) from May 2010 to April 2011. $\delta^{41}K$ values of these samples range from −0.57‰ to −0.34‰. The low $\delta^{41}K$ values were for the May and June samples, whereas the remaining samples have consistent and higher $\delta^{41}K$ values of −0.40‰ to −0.34‰ (Fig. 1). The lack of seasonal variations in riverine dissolved $\delta^{41}K$ is consistent with data from the Fraser River, Canada (24). The lower $\delta^{41}K$ values in the Changjiang River characterize the early part of the wet season, which might be explained by the addition of K with low $\delta^{41}K$ values from plant litter (19, 25, 26). Alternatively, the low $\delta^{41}K$ signatures could be explained by the release of isotopically light K by leaves (19, 25, 26) into throughfall (i.e., the raindrops that penetrate through the canopy and fall onto the soil surface) and subsequently river water via interactions between rainwater and plant canopy (27, 28).

Irrespective of the exact mechanism responsible for the two low $\delta^{41}K$ data points in the time-series data, the overall stability of $\delta^{41}K$ values in the river dissolved load during the rest of the year is clear (Fig. 1). The annual weighted-average $\delta^{41}K$ value of the Changjiang River is −0.41‰ ± 0.07‰, which is within error of >80% of the river samples from that river. Our data indicate that river waters sampled at any time, apart from the early part of the wet season, are representative of the annual riverine K isotopic composition. The following discussion is based on samples that were not collected during the early part of the wet season.

K Isotope Fractionation During Chemical Weathering. Given the relative stability of the K isotopic composition in riverine inputs, we can reasonably evaluate K isotope fractionation during silicate weathering by analyzing river waters and sediments. Seven pairs of river water–sediment samples from two small single-lithology granite watersheds (*SI Appendix*, Fig. S2) were analyzed (Fig. 2). The $\delta^{41}K$ values of these river waters vary from −0.29‰ to +0.03‰ (*SI Appendix*, Table S1). Based on the very low Cl concentrations in rain water, the river samples are essentially free of sea salt contamination (*SI Appendix*), and mass balance calculations indicate that the possible shifts in $\delta^{41}K$ caused by K of marine origin are <0.01‰ (*SI Appendix*, Table S1).

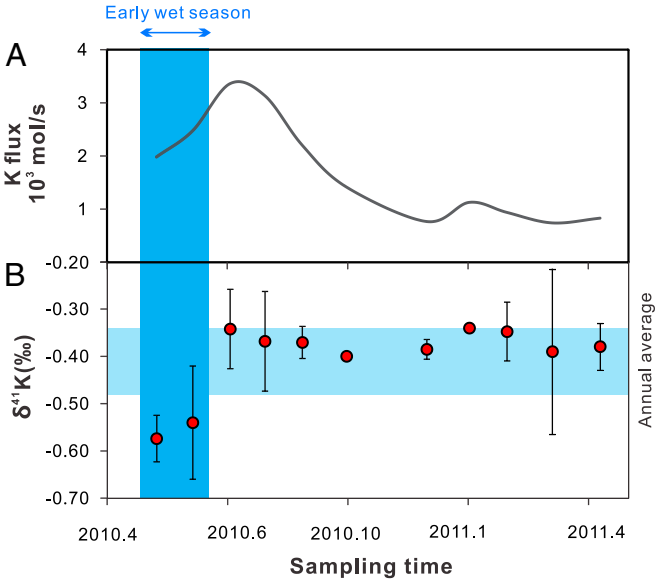

Fig. 1. Seasonal variations in riverine dissolved K flux (*A*) and its $\delta^{41}K$ value (*B*). The dark blue shaded area marks the short interval when $\delta^{41}K$ is relatively low. The light blue shaded area marks the K flux weighted average riverine $\delta^{41}K$ for a hydrological year. Symbols with no error bar have errors that are smaller than the size of the symbol. Samples taken at any time except for the early stage of the wet season are representative of the K flux weighted average $\delta^{41}K$.

The fresh granite bedrock of the catchment yields $\delta^{41}K$ = −0.47‰ ± 0.11‰ (n = 2), which is within error of the bulk silicate Earth (BSE) value of −0.52‰ (18–20). Two sediment size fractions (i.e., the >75-μm coarse and <2-μm clay fractions) were separated and analyzed. $\delta^{41}K$ values of the >75-μm fraction range from −0.68‰ to −0.48‰ (*SI Appendix*, Table S2), which are close to or slightly lower than the values of the bedrock samples. In comparison, $\delta^{41}K$ values of the <2-μm fraction range from −0.74‰ to −0.58‰ (*SI Appendix*, Table S2), which are slightly lower than those of the coarse fraction and bedrock samples.

Unlike sediments in large river basins that could be derived from recycling of old sedimentary rocks (29), the sediments measured here are sampled from small granitic watersheds and are thus derived locally from weathering of the primary igneous rocks. Therefore, the pronounced difference in $\delta^{41}K$ values between the riverine dissolved load and sediments (Fig. 2) provides direct evidence for K isotope fractionation during silicate weathering. Our data show that ^{41}K is preferentially released into solution, whereas ^{39}K is preferentially incorporated into secondary minerals as shown by the low $\delta^{41}K$ values of the clay fraction, driving $\delta^{41}K$ of riverine dissolved loads to values higher than BSE. Based on the assumption that $\delta^{41}K$ values in river water are invariant with time, a K isotope fractionation factor can be derived between clay and water by subtracting the $\delta^{41}K$ value of river water from the $\delta^{41}K$ value of the <2-μm sediment size fraction, giving $\Delta^{41}K_{min-aq}$ = −0.55 ± 0.29‰ (2 SD; n = 7). It should be noted that this is an empirical estimate based on the assumptions that the clay fraction is representative of the solid products of weathering and that the $\delta^{41}K$ of the dissolved load is constant without temporal variations, the latter of which is supported by the Changjiang River data (Fig. 1).

Relationship Between $\delta^{41}K$ Values of Riverine Dissolved Load and Weathering Intensity. We now explore the relationship between the $\delta^{41}K$ values of riverine dissolved load and WI. WI is defined as the mass ratio of the silicate weathering rate (W) to the total

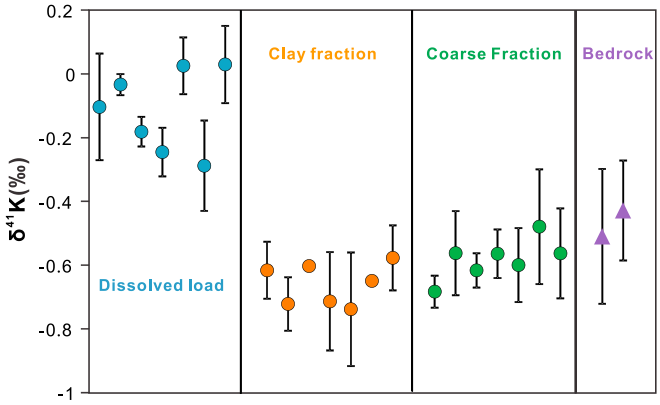

Fig. 2. K isotope composition of the dissolved loads (blue circles), bedrocks (purple triangles), and river sediments that have been size sorted into a clay fraction (orange circles) and a coarser grained fraction (green circles). All samples were taken from watersheds with a granitic bedrock composition.

denudation rate (D), which is the sum of the silicate weathering rate (W) and physical weathering rate (E) (30):

$$WI = W/D = W/(W + E). \quad [1]$$

A dataset of physical erosion rates (E) for the sampled rivers was compiled from the literature (*SI Appendix*, Table S4). For this analysis, it was assumed that the riverine suspended load is equivalent to the physical erosion rate (e.g., refs. 13, 14, and 30). Silicate weathering rates for all of the studied Chinese river basins have been reported in previous studies (31–36), apart from the Minjiang River. We calculated the silicate weathering rate for the Minjiang River using a forward model (*SI Appendix*). The calculated WI ranges from 0.002 to 0.154, reflecting significant differences in the weathering regimes of the studied rivers. In a plot of dissolved $\delta^{41}K$ versus ln(WI), the data points for the rivers with low Cl contents define a linear trend with a negative slope (Fig. 3*A*). Two samples with high Cl contents (>2,000 μmol/L) fall off this trend and have higher $\delta^{41}K$ values. Considering the Cl contributed from atmospheric input is <106 μmol/L (*SI Appendix*), the high Cl concentrations suggest these samples are significantly affected by evaporite dissolution. Therefore, these data outliers may reflect the addition of K from evaporite deposits, which have high $\delta^{41}K$ values (18, 20). On a global scale, the effect of the addition of evaporitic K to the riverine dissolved load is insignificant (17), mainly due to the relatively rare occurrence of potash salts in evaporites (37).

Low $\delta^{41}K$ values were generally observed in the lower reaches of large river basins, where human activity is more intense. One could argue that anthropogenic processes contribute isotopically light K, resulting in riverine dissolved loads having the lower $\delta^{41}K$ values in Fig. 3*A*. However, we reject this hypothesis for three reasons. First, anthropogenic processes greatly influence the riverine NO_3^- budget, and if the $\delta^{41}K$ variations in riverine dissolved loads were driven primarily by anthropogenic processes, we would expect to observe a correlation between NO_3/K ratios and $\delta^{41}K$ values, which was not observed (*SI Appendix*, Fig. S3). Second, the excellent correlation ($R^2 = 0.87$; $n = 12$) (Fig. 3*B*) between $\delta^{41}K$ values of the riverine dissolved load and the chemical index of alteration (CIA) of the river sediments (Fig. 3*B*) suggests that $\delta^{41}K$ is controlled primarily by natural weathering processes. Third, given that potash fertilizers are produced primarily from marine evaporites (38), which have high $\delta^{41}K$ values (18, 20), we would expect higher $\delta^{41}K$ values in river samples affected by agricultural use in lower reaches, where the WI values are generally higher, but this is inconsistent with the negative correlation between $\delta^{41}K$ and WI (Fig. 3*A*). As such, we conclude that enhanced anthropogenic processes in the lower reaches of these large river basins do not significantly change the K isotopic signature of the river water, and thus the negative correlation between $\delta^{41}K$ and WI (Fig. 3*A*) reflects natural weathering processes.

Data from the small granite watersheds strongly suggest that ^{39}K is preferentially incorporated into secondary phases, leaving riverine dissolved loads enriched in ^{41}K. During low-intensity chemical weathering, this mechanism should be the dominant process, as supported by the high $\delta^{41}K$ values of water from low-WI rivers (Fig. 3*A*). In contrast, during high-intensity chemical weathering of silicates, gibbsite and iron oxides are the weathering products (39) and no K is retained in solid phases. Complete dissolution of K-bearing minerals in silicate rocks would result in no net K isotope fractionation, and the $\delta^{41}K$ of riverine dissolved load should be equal to the BSE value (–0.52‰; Fig. 3). The linear trend in Fig. 3*A* is in contrast to the relationship between δ^7Li and ln(WI) reported by Dellinger et al. (13), who found that δ^7Li increases when WI increases from 0.004 to 0.04 but decreases when WI increases to >0.04. The different responses to WI of K and Li isotopes may be due to mineralogical controls (*SI Appendix*) and the fact that K is a major element whereas Li is a trace element. According to the negative correlation between $\delta^{41}K$ and WI (Fig. 3*A*), rivers draining mountainous regions are expected to have higher dissolved $\delta^{41}K$ values because silicate WI is low in regions of higher denudation rates (40), whereas lower $\delta^{41}K$ are expected in rivers draining tectonically stable cratons where denudation rates are low and primary silicate minerals are intensely weathered (30, 41).

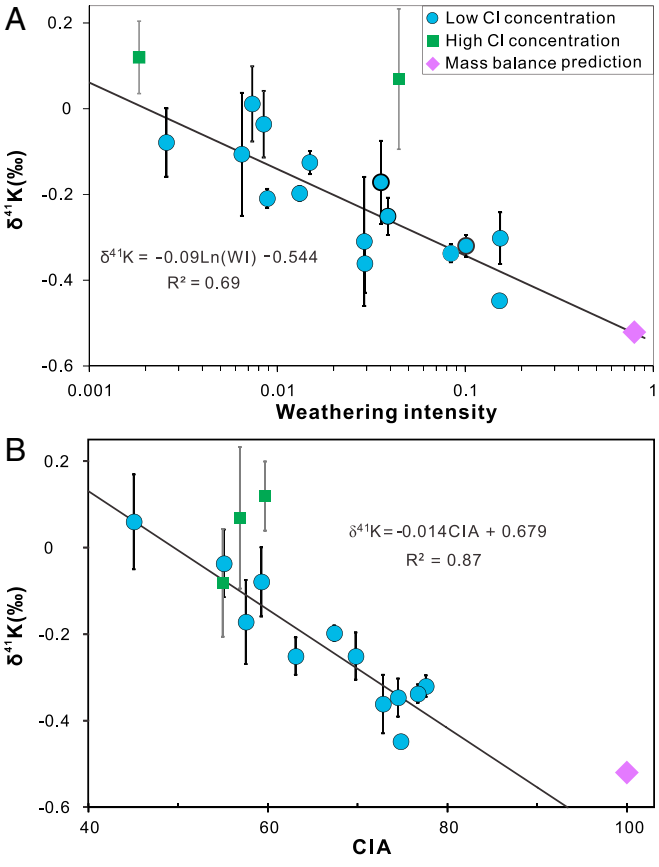

Fig. 3. Cross-plots of $\delta^{41}K$ in riverine dissolved loads versus WI (*A*) and CIA in river sediments (*B*). Symbols with no error bar have errors smaller than the size of the symbol. The mass balance prediction is based on assuming that riverine $\delta^{41}K$ should equal bulk silicate earth at the theoretically highest WI of 0.8 and the highest CIA of 100.

Interestingly, if the linear trend in the plot of $\delta^{41}K$ versus ln(WI) is extrapolated to the highest WI value of 0.8, as calculated from the geochemical composition of upper continental crust (42), a $\delta^{41}K$ value of −0.52‰ is obtained (Fig. 3), which is identical to the BSE value. This implies that the crustal rocks have a BSE-like K isotopic composition when averaged on a basin scale. As the WI decreases from this hypothetical maximum value of 0.8, the weathering congruency decreases. This would lead to preferential retention of light K isotopes in secondary clays and an increase in $\delta^{41}K$ values in riverine dissolved loads, resulting in a negative correlation between ln(WI) and $\delta^{41}K$ values in riverine dissolved loads (Fig. 3*A*). The logarithmic relationship between WI and riverine $\delta^{41}K$ (Fig. 3*A*) provides an approach to estimate the average K isotopic composition of global continental riverine runoff. Using a modern global silicate weathering rate of 5.50×10^8 t/y (43) and a modern physical erosion rate of 1.91×10^{11} t/y (44), the modern global WI is calculated to be 0.029 ± 0.006, considering a 30% uncertainty in the global silicate weathering rate (43) and a 20% uncertainty in the physical erosion rate (45). With this estimate and the regression shown in Fig. 3*A*, the average $\delta^{41}K$ value of global riverine runoff is determined to be −0.22 ± 0.04‰.

Implications for Modern and Ancient Global K Cycling. K stable isotopes offer insights into the global cycling of K, which is poorly understood relative to the cycling of other major elements (46–48). K is added into oceans via riverine runoff (F_{riv}) and midocean ridge hydrothermal fluxes (F_{MOR}) (49, 50), which are balanced by K removal from seawater via neoformation of clays and ion exchange during sediment diagenesis (F_{sed}) and low-temperature basalt alteration (F_{alt}) (48, 51). Large uncertainties, however, exist in estimates for the K fluxes in and out of modern oceans. For example, while the estimates for F_{riv} and F_{alt} are relatively tight within 52 to 60 Tg/y (16, 46, 47) and 12 to 15.6 Tg/y (46, 47), respectively, estimates for F_{MOR} and F_{sed} have a large range, from 5 to 36 Tg/y (46–49, 52) and from 25 to 52 Tg/y (46–48), respectively. The K fluxes associated with sediment diagenesis and low-temperature basalt alteration cannot be precisely calculated using conventional approaches. However, now we can place an additional dimension of constraints on the modern K cycle based on isotope mass balance. K in the oceans is considered to be in a secular steady state (53), and if we further assume a K isotopic steady state for the modern ocean, we have

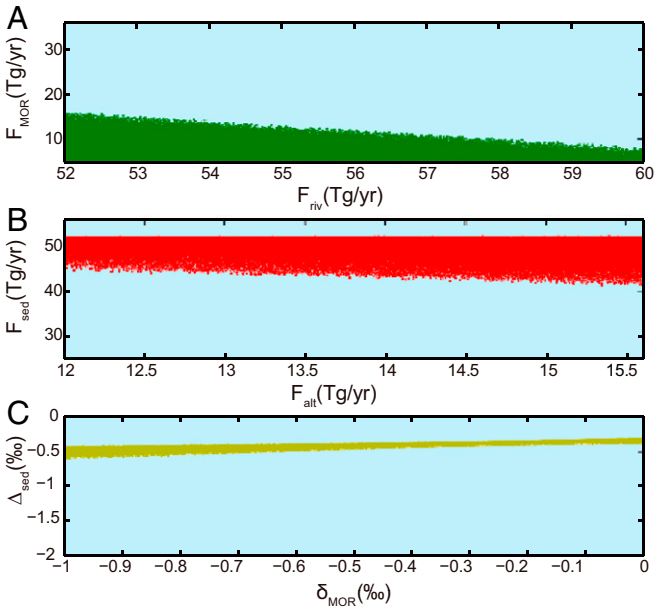

Fig. 4. Cross-plots of F_{riv} versus F_{MOR} (*A*), F_{alt} versus F_{sed} (*B*), and $\delta^{41}K_{MOR}$ versus Δ_{sed} (*C*) for modern global K cycling. The light blue areas present the ranges of F_{riv}, F_{MOR}, F_{alt}, F_{sed}, and Δ_{sed} reported in literature (16, 46–49, 52, 54). The colored spots represent the 57,441 solutions obtained from the Monte Carlo simulation that incorporates mass and isotopic balance of oceanic K cycle.

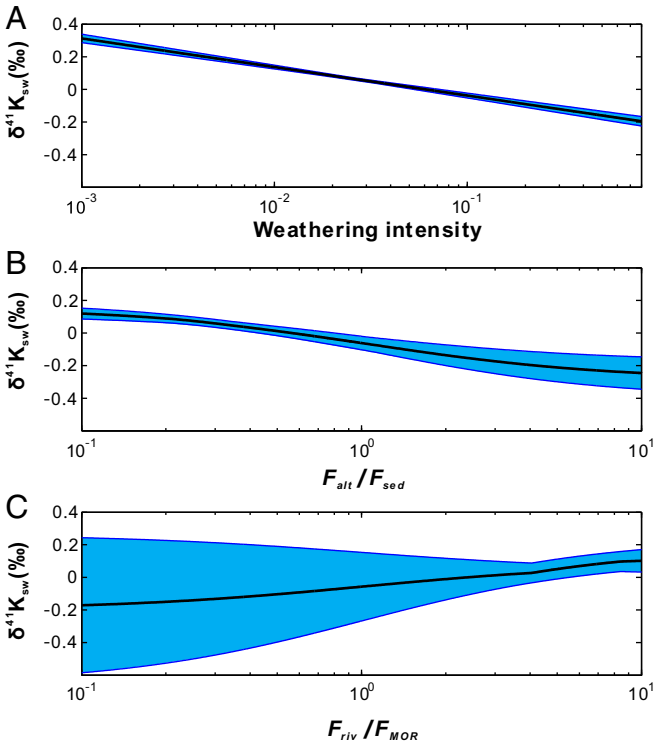

Fig. 5. Sensitivity test of seawater K isotope response to variations in WI (*A*), F_{alt}/F_{sed} ratios (*B*), and F_{riv}/F_{MOR} ratios (*C*). The black curves represent the modeled median values. Blue areas represent the possible range in $\delta^{41}K$ of seawater (i.e., the difference between the highest and lowest values at a given value of WI, F_{alt}/F_{sed}, or F_{riv}/F_{MOR}) considering the uncertainties of F_{riv}, F_{MOR}, F_{alt}, F_{sed}, $\delta^{41}K_{MOR}$, and Δ_{sed} as estimated in the Monte Carlo simulation.

$$F_{riv} + F_{MOR} = F_{sed} + F_{alt} \quad [2]$$

$$\delta_{riv}F_{riv} + \delta_{MOR}F_{MOR} = (\delta_{sw} + \Delta_{sed})F_{sed} + (\delta_{sw} + \Delta_{alt})F_{alt}, \quad [3]$$

where F and δ represent the K fluxes and isotopic compositions of the four major components of global K cycling mentioned above. Δ denotes the K isotope fractionation factor for low-temperature alteration of basalt (alt) or sediment diagenesis (sed). Δ_{sed} has recently been estimated to range from −2 to 0‰ based on model fitting of $\delta^{41}K$ values from pore water obtained from several Integrated Ocean Drilling Program drill cores (54). Δ_{alt} is inferred to be ~0‰ based on a study on basalts altered at low temperatures (22). δ_{sw} is +0.06‰ (19) and δ_{riv} is −0.22‰ based on this study. Since there has been no report on δ_{MOR}, we conservatively set a large range of −1 to 0‰ for δ_{MOR}.

Eqs. **2** and **3** contain many variables with large uncertainties, but these uncertainties can be significantly reduced if both elemental and isotopic mass balances are considered. We applied a Monte Carlo approach (*SI Appendix*, Fig. S6) to address the problem, by using random values from the reported ranges for the parameters then testing whether the random value sets simultaneously satisfy Eq. **2** and Eq. **3**. We ran the Monte Carlo model 2.4 billion times and obtained 57,441 solutions. Tests

show that the full range of all possible combinations of parameters has been thoroughly explored after 0.5 billion Monte Carlo simulations (*SI Appendix*, Fig. S7).

The solutions from the Monte Carlo simulation are shown in Fig. 4. It is clear that the uncertainties in F_{MOR} and F_{sed} are greatly reduced compared with the large range of estimates in previous studies (16, 46–49, 52). Modern F_{MOR} and F_{sed} are now constrained to be within 5 to 15.8 Tg/y and 41 to 52 Tg/y, respectively. However, the results show that the mass balance models are insensitive to the existing uncertainties in F_{riv}, F_{alt}, and δ_{MOR}, and therefore we cannot improve on these estimates. The modeling also dramatically reduces the uncertainty in Δ_{sed}, down from a range of −2 to 0‰ (54) to −0.6 to −0.3‰. Δ_{sed} should be primarily associated with clay formation as it is the dominant process for K consumed by sediment diagenesis (47, 48), and the K isotope fractionation factor for clays inferred from the <2-μm sediment size fraction from the granite watersheds in this study is −0.55 ± 0.29‰ (Fig. 2). The consistency between the K isotope fractionation factors from two independent methods supports the validity of the Monte Carlo simulations.

We now consider the response of seawater $\delta^{41}K$ to the possible changes in the global cycling of K in geological history. In previous sections, we have shown that riverine $\delta^{41}K$ value is variable and dependent on WI; therefore, continental WI could be one of the controlling factors of seawater $\delta^{41}K$. To test the effects of K cycling on seawater $\delta^{41}K$, we calculate seawater $\delta^{41}K$ as a function of changes in K sinks, K sources, and WI. The changes in K sinks are presented as changes in ratios of F_{alt} over F_{sed} (F_{alt}/F_{sed}) and the changes in K sources are represented by ratios of F_{riv} to F_{MOR} (F_{riv}/F_{MOR}). Combing Eq. **2** with Eq. **3** and solving for $\delta^{41}K_{sw}$, we have

$$\delta^{41}K_{sw} = (\delta_{riv}F_{riv}/F_{MOR} + \delta_{MOR})/(F_{riv}/F_{MOR} + 1) - \Delta_{sed}/(F_{alt}/F_{sed} + 1). \quad [4]$$

The sensitivity of $\delta^{41}K_{sw}$ to the different factors is tested using a single-variant approach. In the sensitivity tests for WI, F_{riv}/F_{MOR}, or F_{alt}/F_{sed}, we let WI, F_{riv}/F_{MOR}, or F_{alt}/F_{sed} increase from 0.001 to 0.8, from 0.1 to 10, and from 0.1 to 10, respectively. Meanwhile, the rest of the parameters in Eq. **4** are set to the values derived from the 57,441 solutions obtained by the Monte Carlo calculations. In this way, we can evaluate the variability of $\delta^{41}K_{SW}$ values at a given value of the variable brought by the uncertainties associated with the fluxes and isotope compositions constrained by our Monte Carlo simulations. The results are present as median ± ½ range in Fig. 5. The range here is the difference between the lowest and highest values of $\delta^{41}K_{sw}$ at a given value of the variable.

The results show that if F_{alt}/F_{sed} and F_{riv}/F_{MOR} ratios are constant, $\delta^{41}K_{sw}$ would decrease from 0.31 ± 0.03‰ to −0.20 ± 0.03‰ when WI increases from 0.001 to 0.8; if WI and F_{riv}/F_{MOR} are constant, $\delta^{41}K_{sw}$ would decrease from 0.12 ± 0.03‰ to −0.25 ± 0.10‰ when F_{alt}/F_{sed} increases from 0.1 to 1. These predicted variations are relatively small and will require high-precision K isotope analyses to resolve. Sensitivity tests also show that $\delta^{41}K_{sw}$ increases with increasing F_{riv}/F_{MOR} values, despite the significant uncertainty at low F_{riv}/F_{MOR} values due to the large uncertainties in δ_{MOR}. Because clay formation in ocean sediments requires an input of Al and Si from continental runoffs (55), F_{alt}/F_{sed} should be negatively correlated with the relative strength of continental weathering over midocean ridge activity, as F_{riv}/F_{MOR} does.

In summary, these sensitivity tests collectively indicate that K isotopes in seawater can be a useful proxy of continental weathering over geological history. Furthermore, recent experimental work has shown that there is no K isotope fractionation between aqueous K and sylvite (23), and therefore it should be possible to reconstruct the $\delta^{41}K_{sw}$ for ancient oceans based on high precision analysis of suitable evaporite records containing primary sylvite. Future studies of the high precision seawater $\delta^{41}K$ records will improve our understanding of the interplay between mountain building, weathering, carbon cycling, and climate throughout Earth's history.

Materials and Methods

Sample Preparation. We sampled a number of Chinese rivers and also two small streams draining granites at the Jiangxi and Anhui provinces in China. During sampling, about 2 L of river water was transferred to acid-washed low-density polyethylene bottles. Five milliliters of the water sample was used for dissolved inorganic carbon concentration measurement by HCl titration, with an uncertainty of ±5%. The rest of the water sample was filtered through a 0.22-μm cellulose acetate membrane and the first 300 mL water was discarded to minimize contamination from filtration. The remaining sample was acidified to pH = 2 using ultrapure-grade nitric acid.

Seven riverine sediment samples were collected in the small granite watershed. The >75-μm fraction (coarse fraction) was extracted by sieving the ultrasonically dispersed samples in MQ water and the <2-μm fraction (clay fraction) was separated and recovered by centrifuging using the suspended solutions according to the Stokes' law, that the travel speed of the particles in water depends on their sizes.

K Isotope Analysis. For K isotope analysis, solid samples were digested using a mixture of 1 mL HNO_3 and 0.5 mL HF in a capped Teflon beaker and heated at 130 °C overnight. The sample was then dried down at 95 °C. For riverine dissolved samples, 20 mL of river water was evaporated to dryness. Both types of samples were refluxed in concentrated nitric acid overnight. This process was repeated three times to transform all of the dissolved salts into nitrates. Then the sample was redissolved in 0.5 mL 1.5 mol/L HNO_3 and prepared for column chemistry. K was purified using an established two-stage column procedure (19), first on an AG50WX12 column and then on an AG50WX8 column. K isotope ratios are measured using a collision-cell–equipped single-focusing multicollector inductively coupled plasma mass spectrometer at the University of Wisconsin–Madison. The long-term external reproducibility is ±0.19‰ (2 SD). The accuracy of our measurement is done by measuring synthetic samples made by mixing NIST 3141a K standard with K-free matrix elements separated from various geological samples used in this study. The $\delta^{41}K$ values of the six synthetic samples are −0.04 ± 0.06‰ (n = 6), thus proving the accuracy of our measurement.

ACKNOWLEDGMENTS. We thank Matthew Brzozowski for assistance in proofreading the manuscript and Jérôme Gaillardet and two anonymous reviewers for constructive reviews. This work was supported by National Key R&D Program of China Project 2017YFC0602801 and National Science Foundation of China Grants 41622301, 41873004 (to W.L.), and 41730101 (to J.C.). The work done at the University of Wisconsin was in part supported by NASA Astrobiology Institute Grant NNA13AA94A (to B.L.B.) and National Science Foundation Grant 1741048-EAR (to B.L.B.).

1. Raymo ME, Ruddiman WF (1992) Tectonic forcing of late Cenozoic climate. *Nature* 359:117–122.
2. Raymo ME, Ruddiman WF, Froelich PN (1988) Influence of late Cenozoic mountain building on ocean geochemical cycles. *Geology* 16:649–653.
3. Berner RA, Lasaga AC, Garrels RM (1983) The carbonate-silicate geochemical cycle and its effect on atmospheric carbon dioxide over the past 100 million years. *Am J Sci* 283: 641–683.
4. Misra S, Froelich PN (2012) Lithium isotope history of Cenozoic seawater: Changes in silicate weathering and reverse weathering. *Science* 335:818–823.
5. Swanson-Hysell NL, Macdonald FA (2017) Tropical weathering of the Taconic orogeny as a driver for Ordovician cooling. *Geology* 45:719–722.
6. Blum JD, Gazis CA, Jacobson AD, Chamberlain CP (1998) Carbonate versus silicate weathering in the Raikhot watershed within the High Himalayan Crystalline Series. *Geology* 26:411–414.
7. Jacobson AD, Blum JD (2000) Ca/Sr and 87Sr/86Sr geochemistry of disseminated calcite in Himalayan silicate rocks from Nanga Parbat: Influence on river-water chemistry. *Geology* 28:463–466.
8. Pegram WJ, Krishnaswami S, Ravizza GE, Turekian KK (1992) The record of sea water 187Os/186Os variation through the Cenozoic. *Earth Planet Sci Lett* 113:569–576.
9. Crusius J, Calvert S, Pedersen T, Sage D (1996) Rhenium and molybdenum enrichments in sediments as indicators of oxic, suboxic and sulfidic conditions of deposition. *Earth Planet Sci Lett* 145:65–78.

10. Ravizza G, Esser BK (1993) A possible link between the seawater osmium isotope record and weathering of ancient sedimentary organic matter. *Chem Geol* 107: 255–258.
11. Peucker-Ehrenbrink B, Ravizza G (2000) The marine osmium isotope record. *Terra Nova* 12:205–219.
12. Torres MA, West AJ, Li G (2014) Sulphide oxidation and carbonate dissolution as a source of CO2 over geological timescales. *Nature* 507:346–349.
13. Dellinger M, et al. (2015) Riverine Li isotope fractionation in the Amazon River basin controlled by the weathering regimes. *Geochim Cosmochim Acta* 164:71–93.
14. Dellinger M, Bouchez J, Gaillardet J, Faure L, Moureau J (2017) Tracing weathering regimes using the lithium isotope composition of detrital sediments. *Geology* 45: 411–414.
15. Peizhen Z, Molnar P, Downs WR (2001) Increased sedimentation rates and grain sizes 2-4 Myr ago due to the influence of climate change on erosion rates. *Nature* 410: 891–897.
16. Berner EK, Berner RA (2012) *Global Environment: Water, Air, and Geochemical Cycles* (Princeton Univ Press, Princeton).
17. Meybeck M (1987) Global chemical weathering of surficial rocks estimated from river dissolved loads. *Am J Sci* 287:401–428.
18. Morgan LE, et al. (2018) High-precision $^{41}K/^{39}$ K measurements by MC-ICP-MS indicate terrestrial variability of δ^{41}K. *J Anal At Spectrom* 33:175–186.
19. Li W, Beard B, Li S (2016) Precise measurement of stable potassium isotope ratios using a single focusing collision cell multi-collector ICP-MS. *J Anal At Spectrom* 31: 1023–1029.
20. Wang K, Jacobsen SB (2016) An estimate of the Bulk Silicate Earth potassium isotopic composition based on MC-ICPMS measurements of basalts. *Geochim Cosmochim Acta* 178:223–232.
21. Hu Y, Chen X-Y, Xu Y-K, Teng F-Z (2018) High-precision analysis of potassium isotopes by HR-MC-ICPMS. *Chem Geol* 493:100–108.
22. Parendo CA, Jacobsen SB, Wang K (2017) K isotopes as a tracer of seafloor hydrothermal alteration. *Proc Natl Acad Sci USA* 114:1827–1831.
23. Li W, Kwon KD, Li S, Beard BL (2017) Potassium isotope fractionation between K-salts and saturated aqueous solutions at room temperature: Laboratory experiments and theoretical calculations. *Geochim Cosmochim Acta* 214:1–13.
24. Lee HL, Peucker-Ehrenbrink B, Chen H, Hasenmueller EA, Wang K (2018) Potassium isotopes in major world rivers: Implications for weathering and the seawater budget. Available at https://goldschmidtabstracts.info/2018/1434.pdf (abstr).
25. Li W (2017) Vital effects of K isotope fractionation in organisms: Observations and a hypothesis. *Acta Geochimica* 36:374–378.
26. Christensen JN, Qin L, Brown ST, DePaolo DJ (2018) Potassium and calcium isotopic fractionation by plants (soybean [Glycine max], rice [Oryza sativa], and wheat [Triticum aestivum]). *ACS Earth Space Chem* 2:745–752.
27. Likens GE, et al. (1994) The biogeochemistry of potassium at Hubbard Brook. *Biogeochemistry* 25:61–125.
28. Riotte J, et al. (2014) Vegetation impact on stream chemical fluxes: Mule Hole watershed (South India). *Geochim Cosmochim Acta* 145:116–138.
29. Dellinger M, et al. (2014) Lithium isotopes in large rivers reveal the cannibalistic nature of modern continental weathering and erosion. *Earth Planet Sci Lett* 401: 359–372.
30. Bouchez J, Gaillardet J, von Blanckenburg F (2014) Weathering intensity in lowland river basins: From the Andes to the Amazon mouth. *Procedia Earth Planet Sci* 10: 280–286.
31. Chetelat B, et al. (2008) Geochemistry of the dissolved load of the Changjiang basin rivers: Anthropogenic impacts and chemical weathering. *Geochim Cosmochim Acta* 72:4254–4277.
32. Hren MT, Chamberlain CP, Hilley GE, Blisniuk PM, Bookhagen B (2007) Major ion chemistry of the Yarlung Tsangpo–Brahmaputra river: Chemical weathering, erosion, and CO 2 consumption in the southern Tibetan plateau and eastern syntaxis of the Himalaya. *Geochim Cosmochim Acta* 71:2907–2935.
33. Noh H, Huh Y, Qin J, Ellis A (2009) Chemical weathering in the three rivers region of Eastern Tibet. *Geochim Cosmochim Acta* 73:1857–1877.
34. Sun H, Han J, Li D, Zhang S, Lu X (2010) Chemical weathering inferred from riverine water chemistry in the lower Xijiang basin, South China. *Sci Total Environ* 408: 4749–4760.
35. Wu W, Yang J, Xu S, Yin H (2008) Geochemistry of the headwaters of the Yangtze River, Tongtian He and Jinsha Jiang: Silicate weathering and CO_2 consumption. *Appl Geochem* 23:3712–3727.
36. Wu W, Xu S, Yang J, Yin H (2008) Silicate weathering and CO_2 consumption deduced from the seven Chinese rivers originating in the Qinghai-Tibet Plateau. *Chem Geol* 249:307–320.
37. Babel M, Schreiber B (2014) Geochemistry of evaporites and evolution of seawater. *Treatise on Geochemistry: Sediments, Diagenesis, and Sedimentary Rocks*, ed Mackenzie F (Elsevier, Amsterdam), 2nd Ed, Vol 9, pp 483–560.
38. Fite RC (1951) Origin and occurrence of commercial potash deposits. *Proceedings of the Oklahoma Academy of Science* (Oklahoma Academy of Science, Oklahoma City, OK), pp 123–125.
39. Eggleton R (2001) *The regolith glossary—Surficial geology, soils and landscapes* (Cooperative Research Centre for Landscape Evolution and Mineral Exploration, Millaa Millaa, QLD, Australia).
40. West AJ, Galy A, Bickle M (2005) Tectonic and climatic controls on silicate weathering. *Earth Planet Sci Lett* 235:211–228.
41. Stallard R, Edmond J (1983) Geochemistry of the Amazon: 2. The influence of geology and weathering environment on the dissolved load. *J Geophys Res Oceans* 88: 9671–9688.
42. Gao S, et al. (1998) Chemical composition of the continental crust as revealed by studies in East China. *Geochim Cosmochim Acta* 62:1959–1975.
43. Gaillardet J, Dupré B, Louvat P, Allegre C (1999) Global silicate weathering and CO_2 consumption rates deduced from the chemistry of large rivers. *Chem Geol* 159:3–30.
44. Milliman J, Farnsworth K (2011) *River Discharge to the Coastal Ocean: A Global Synthesis* (Cambridge Univ Press, Cambridge, UK).
45. von Blanckenburg F, Bouchez J (2014) River fluxes to the sea from the ocean's $^{10}Be/^{9}Be$ ratio. *Earth Planet Sci Lett* 387:34–43.
46. Jarrard RD (2003) Subduction fluxes of water, carbon dioxide, chlorine, and potassium. *Geochem Geophys Geosyst* 4:8905.
47. Holland HD (2005) Sea level, sediments and the composition of seawater. *Am J Sci* 305:220–239.
48. Bloch S, Bischoff JL (1979) The effect of low-temperature alteration of basalt on the oceanic budget of potassium. *Geology* 7:193–196.
49. Elderfield H, Schultz A (1996) Mid-ocean ridge hydrothermal fluxes and the chemical composition of the ocean. *Annu Rev Earth Planet Sci* 24:191–224.
50. Garrels R, Mackenzie FT (1971) *Evolution of Sedimentary Rocks* (Norton, New York).
51. Kronberg BI (1985) Weathering dynamics and geosphere mixing with reference to the potassium cycle. *Phys Earth Planet Inter* 41:125–132.
52. Staudigel H (2014) Chemical fluxes from hydrothermal alteration of the oceanic crust. *Treatise on Geochemistry*, eds Holland HD, Turekian KK (Elsevier, Amsterdam), 2nd Ed, Vol 4, pp 583–606.
53. Horita J, Zimmermann H, Holland HD (2002) Chemical evolution of seawater during the Phanerozoic: Implications from the record of marine evaporites. *Geochim Cosmochim Acta* 66:3733–3756.
54. Ramos DPS, Morgan LE, Lloyd NS, Higgins JA (2018) Reverse weathering in marine sediments and the geochemical cycle of potassium in seawater: Insights from the K isotopic composition (41K/39K) of deep-sea pore-fluids. *Geochim Cosmochim Acta* 236:99–120.
55. Mackenzie FT, Kump LR (1995) Reverse weathering, clay mineral formation, and oceanic element cycles. *Science* 270:586–587.